Journal of Physical Chemistry and Functional Materials

Home Page of Journal: https://dergipark.org.tr/jphcfum

Visible Light Induced Photocatalytic Removal of Methylene Blue Using Cu-Tunable p-type ZnO Nanoparticles

Auwal Yushau, Abdullahi Muhammad, Kamaludeen Sulaiman Kabo

Department of Applied Chemistry, Faculty of Physical Science, Federal University Dutsin-Ma, P. M. B 5001, Katsina State, Nigeria
** Corresponding author: Auwal Yushau Email: auwalyushau2018@gmail.com*

ABSTRACT

Removal of phototoxicity and zootoxicity pollutants from the aqueous environment is of great importance to human and aquatic life. Copper-tunable p-type zinc oxide (Cu-ZnO) photocatalysts have been prepared by the chemical co-precipitation method. The structural, morphological, elemental and optical properties of the obtained catalysts were characterized using x-ray diffraction (XRD), scanning electron microscopy (SEM), energy dispersive x-ray (EDX) analysis and ultraviolet-visible (UV-Vis) spectrophotometry. The diffraction patterns of the as-synthesized catalysts were matched with that of the hexagonal wurtzite structure for the standard ZnO nanoparticles. The photocatalytic activity of the prepared Cu-doped ZnO catalyst was evaluated using methylene blue (MB) dye under various conditions. The effect of operational parameters such as MB initial concentration, catalyst dosage, and solution pH was optimized using a face central composite design (FCCD) of the response surface methodology (RSM). The optimum photodegradation efficiency of 98.00% was found at 0.30g/L catalyst dose, 10.00mg/L initial concentration of MB and initial pH at 6.00. The degradation model was statistically remarkable with $p < 0.0001\%$ in which the MB initial concentration and solution pH were the most significant variables influencing the removal of MB over the Cu tunable p-type ZnO photocatalyst under visible light irradiation. Finally, the photocatalytic degradation of MB using the undoped and Cu-doped ZnO nanoparticles was nicely fitted pseudo-first-order kinetics scheme.

ARTICLE INFO

Keywords:

Photocatalysis
Cu-tunable p-type ZnO
Visible light
Response Surface Methodology
Kinetics and Methylene Blue

Received: 2023-06-29
Accepted: 2023-07-01
ISSN: 2651-3080
DOI: 10.54565/jphcfum.1321022

1. Introduction

Water pollution is the introduction of unwanted substances into the aqueous environment [1-4]. The harmful substances are called pollutants and they caused sufficient negative effects on aquatic and human life [5-7]. Currently, the aquatic environment is highly polluted by the azo-organic dyes and thus about 60-70% of all the dyes in industry are azo-dyes [8]. Azo dyes are organic compounds that contain the functional group of $R-N=N-R^{I}$, in which R and R^{I} are usually non-azo alkyl or aryl radicals [6]. Methylene Blue (MB) is a cationic heterocyclic aromatic chemical compound with the molecular formula of $C_{16}H_{18}N_3SCl$ and recently, considered as one of the forefront pollutants that belongs to azo-organic dyes [9-12]. However, some of its adverse effects include difficulties in breathing, vomiting, diarrhea, chest pain, mild haemolysis, gastrointestinal disturbance [13, 14]. On the other hand, MB is used widely in the textiles, paints, soaps, and ceramics and pharmaceuticals industries as the coloring materials of their final products [15-17]. These industries however, released their toxic and potential carcinogenic substances into the aqueous ecosystem and thus created severe environmental problems [18, 19]. Nowadays, the removal of MB effluents from the wastewater is of great importance for human safe and aquatic life. As such various physical and chemical methods like adsorption, air stripping, flocculation, precipitation, reverse osmosis, and ultra-filtration for MB removal from the textile effluents have been reported [20-23]. However, the removal of MB effluents by adsorption [24], flocculation [25] and biodegradation [26] have been reported the poor success due to large molecular structure, high solubility, non-biodegradability and requires extra planning [27-29]. Derakhshan *et al.* [30] reported that a degradation efficiency of 58.7% for the adsorption of methylene blue in water over the modified pumice stone. Similarly, Tover *et al* [31] investigated that the bioremoval efficiency of 70% for the bio-removal of the methylene blue from aqueous solution by using galactomyces geotrichum

KL20A. Therefore, more efficient method is highly needed that would improve the removal of MB effluents from the aqueous ecosystem.

Recently, photocatalysis is now attracted the attention of many researchers and widely used as an alternative method for the degradation of all hazardous pollutants due its low cost, excellent photoefficiency, absence of secondary sludge and complete mineralization [32, 33]. The process, however, involves the uses of electromagnetic radiation and semiconductor material known as photocatalyst to drives various photochemical processes. Different metal oxides and sulfides semiconductor such as TiO_2, ZrO_2, WO_3, SnO_2, Fe_2O_3, CdO, ZnS, and CdS have been studied and used as photocatalysts [34-38,]. Zinc oxide (ZnO) photocatalyst is a well-known candidate that extensively used in the degradation of pollutants due to its low cost, non-toxiciy, availability, high spectral ability and stability in nature [39]. On the other hand, the photocatalytic activity of ZnO catalyst is suffered by its inability to absorb the visible light because of its wide band gap (3.26eV). To improve its spectral response to visible light, different approaches such as coupling, dye sensitization, and impregnation have been employed [40]. However, these approaches demonstrated inferior removal efficiency of MB. Therefore, a more operative way to improve the physical, chemical properties and band gap of ZnO catalysts is highly needed.

Doping is now recognized as a one of the most important approaches for the band gap modification of ZnO nanoparticles. The method is intensively used to shift band wavelength from the ultraviolet to the visible light region of the solar spectrum [41]. Different metals such as Mn [42], Mg [43], Al [44], Ga [45], Fe [46], Na [47], Ag [48], Cr [49], Ti [50] and K [51] have been demonstrated to enhance the photoefficiency of the catalyst in the literature. Among the metal dopants copper (Cu) is prefered due to its luminescence enhancement, electronic shell structure, similar chemical and physical properties to Zn and inducing high change in microstructure and optical properties of ZnO photocatalyst [52]. Copper tunable *p*-type zinc oxide (Cu-ZnO) nanoparticles is an excellent visible light photoresponsive catalyst that is widely used in magnetic, photoelectrical and photocatalysis applications. Previous works were reported a better significant success for the degradation of pollutants over the Cu-doped ZnO photocatalyst [53-56]. Biruktait *et al*. [57] were reported the biogenic synthesis of Cu-doped ZnO photocatalyst for the removal of organic dye and the results showed that 89% of the MB was degraded. Ridwan *et al*. [58] were studied the hydrothermal synthesis of vertically aligned Cu-doped ZnO nanorods for photocatalytic activity of enhancement and the responses revealed that 97% of the methylene blue was degraded under 30W UV exposure. Ahmad *et al* [59] were investigated the green synthesis of doped and undoped ZnO nanoparticles for the degradation of industrial dye and the outcomes demonstrated that 74% and 57% of the MB was degraded under UV and visible light irradiation respectively. Awais *et al* [60] revealed the hydrothermal synthesis of Cu-doped ZnO nanoparticles for the removal of organic wastewater and the responses showed that 94% of the MB was degraded in 2 hrs. Nouasria *et al.* [61] were reported the electrodeposition synthesis of Cu-doped ZnO photocatalyst for the degradation of methylene blue (MB), methylene orange (MO) and congo red (CR) and the results showed a significant success under the UV and the natural sunlight illumination. Aqeel *et al*. [62] were studied a facile synthesis of Cu-doped ZnO nanorods for the efficient photodegradation of methylene blue and methyl orange and the outcomes showed that 57.5% and 60% of the MO and MB were degraded at 180 min, respectively. Similarly, Sini *et al*. [63] investigated a facile wet synthesis of Cu-doped ZnO nanostructures for highly efficient photocatalytic degradation of organic dyes and significant responses were obtained for the removal of MB and MO.

Herein, we aim to report the chemical co-precipitation synthesis of Cu-tunable *p*-type ZnO nanoparticles and optimize the process parameters such as initial concentration of MB, catalysts dosage and initial pH of solution using a face central composite design (FCCD) of the response surface methodology (RSM).

2. Experimental Methods

2.1. Materials

Some of the chemicals required in this research work includes zinc sulphate heptahydrate ($ZnSO_4.7H_2O$, 97%), copper sulphate hexahydrate ($CuSO_4.6H_2O$, 98%), hydrochloric acid (HCl, 98%) and methylene blue ($C_{16}H_{18}N_3SCl$, 98%) were supplied by Sigma Aldrich Canada while potassium hydroxide (KOH, 98%) and ammonium hydroxide (NH_4OH, 98%) were obtained from BDH, Poole, England, ammonium oxalate (AO) (97%), *t*-butanol (98%) and *p*-benzoquinoline(98%) supplied by Sigma Aldrich Canada. All these chemicals were of analytical grade. The structural formula of MB is shown in Fig. 1.

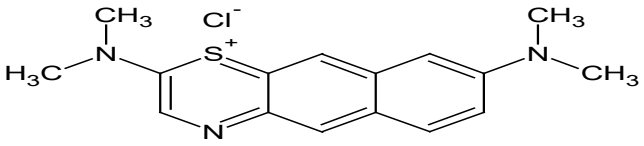

Fig. 1. Molecular structure of MB.

2.2. Synthesis of Cu-tunable *p*-type ZnO Nanoparticles (NPs)

The Cu-tunable *p*-type ZnO nanoparticle was synthesized by the chemical co-precipitation method. The doping of ZnO with Cu was carried out using 80% zinc sulphate heptahydrate ($ZnSO_4.7H_2O$) and 20% copper sulphate hexahydrate ($CuSO_4.6H_2O$) by weight. 0.3M of $CuSO_4.6H_2O$ was dissolved in 400 ml of deionized water under vigorous stirring till a homogeneous solution was obtained. Then an aqueous solution of potassium hydroxide (KOH) (0.5M) were added at a constant rate to the solution with vigorous stirring at room temperature until the pH of the solution reached to 9. The resulting precipitate was aged for 24 h, recovered by centrifugation, washed several times with deionized water until the pH was 7. The sample was dried overnight in an oven at 140 ℃ and then finally it was calcined at 500 ℃ for 4 h in a muffle furnace to obtain a Cu-tunable *p*-type ZnO photocatalyst. While the undoped ZnO nanoparticles was

prepared via the same method but without the addition of copper sulphate. The reactions that involved during the synthesis of Cu-doped ZnO and undoped ZnO photocatalysts are represented in the equations 1 and 2 respectively.

$ZnSO_4.7H_2O + CuSO_4.6H_2O + 2KOH \rightarrow$ Cu-ZnO + 2K + $2SO_4 + 14H_2O$ (1)

$ZnSO_4.7H_2O + 2KOH \rightarrow ZnO + 2K + SO_4 + 8H_2O$ (2)

2.3. Characterization of Bare ZnO and Cu-tunable *p*-type ZnO NPs

The study of structural properties of the synthesized photocatalysts were conducted by x-ray diffraction (XRD) analysis using a Philips Xpert Pro diffractometer operated with a CuK_α radiation (λ= 1.54468 Å) in the 2θ range 5-70 ° at 30 kV, 30 mA and scanning rate of 2 min. The lattice parameters such as spacing distance between the adjacent planes in the miller indices d_{hkl}, lattice constant a, b and c, and volume of the unit cell for the Cu-ZnO and ZnO catalysts were calculated using Eqs. (3-6). The calculated values for the synthesized catalysts were compared to the unit cell parameters for the standard Cu-doped ZnO (JCPDS 070-8073) and undoped ZnO (JCPDS 071-6426).

$$a = b = \frac{\lambda}{\sqrt{3}\sin\theta 001} \quad (3)$$

$$c = \frac{\lambda}{\sin\theta 101} \quad (4)$$

$$d_{hk} = \frac{ac}{2}\sqrt{\frac{3}{c^2\left(h^2 + hk + k^2 + 3\left(\frac{al}{4}\right)2\right)}} \quad (5)$$

$$V = 0.866 \times a^2 \times c \quad (6)$$

Where constants a, b, and c, are the lattice constants, λ is the wavelength of x-ray radiation (1.5406 Å), θ is the Bragg's angle, d_{hkl} is the spacing distance, V is the volume of the unit cell and hkl is the miller indices.

The average particles size has been estimated using Debye-Scherer (Eq. 7). The surface areas for the undoped ZnO and the Cu-doped ZnO were calculated from the eqs. (7-9), respectively.

$$D = \frac{k\lambda}{\beta\cos\theta} \quad (7)$$

$$SSA = \frac{S.A}{V\times\rho} \quad (8)$$

$$SSA = \frac{6000}{D\times\rho} \quad (9)$$

Where D is the average particle size, k is the Debye-Scherer constant (0.89), λ is the wavelength of the x-ray radiation, β is the full width of half maximum intensity (FWHM), θ is the diffraction angle at the position of peak maximum, SSA is the specific surface area, SA is the surface area, ρ is the density of ZnO (5.70 gcm^{-3}) and Cu-doped ZnO (5.68 gcm^{-3})

The surface morphology of the synthesized photocatalysts was recorded on LEICA Stereo scan-440 interfaced with a Phoenix proxy energy dispersive x-ray spectrometer. The facility was operated at the same scale (30 µm), magnification (2,500) and accelerating voltage (15 kV). The elemental composition for the undoped and Cu-doped ZnO photocatalysts was recorded using an E-max-60 spectrometer interfaced with SEM. The band gap values of the catalysts were calculated using Schuster-Kubelka-Munk relation (Eq. 10) from the electronic data recorded over wavelength range 200-800 nm on the Lambda 35 Perkin Elmer UV-Visible spectrophotometer.

$$(\alpha h\nu)^{\frac{1}{n}} = K(h\nu - E_g) \quad (10)$$

Where α is the absorption coefficient obtained from Beer's law, h is the planck's constant, ν is the frequency of vibration, K is the proportionality constant and E_g is the band gap energy of the semiconductor photocatalyst. The E_g values were calculated from the intersect of the plot $(\alpha h\nu)^{\frac{1}{n}}$ against hν.While the K was calculated from the slope. However, if scattering is insignificant the term αhν is proportional to a function of reflectance[$F(R)(\alpha h\nu)$]. Since the semiconductor ZnO used in this experiment is a direct band gap allowed sample transition and thus the denominator of the exponent n = ½.

2.4 Preparation of Methylene Blue Solution

Stock solution of MB was prepared by dissolving 1.0g of commercially available methylene blue in 1.0 Liter of deionized water to obtain a stock concentration of 1000mg/L. Experimental MB solutions of desired concentrations (5, 10, 15, 20, 25 and 30mg/L) were prepared by appropriate dilution of the mother solution.

2.5. Photoxperiments

Photocatalytic performance of the bare ZnO and Cu tunable *p*-type ZnO nanoparticles were studies for the removal of methylene blue (MB). All experiments were carried out in a 30 cm long, 1 liter capacity, round bottom batch photoreactor which was maintained at 298K. The visible light source was a 300W Xenon lamp emitting at 400 nm. This lamp was jacketed in cylindrical quartz glass, dipping down the photoreactor [64] bottom.

Specifically, 500 ml aqueous solution of the desired amount of MB (10-30mg/L) and Cu-doped ZnO photocatalyst (0.1-0.6g) were added to the photoreactor and the pH of the suspension was adjusted using 0.1 $molL^{-1}$ NH_4OH and HCl. This mixture was magnetically stirred for 25 min in the dark to establish adsorption equilibrium, and then exposed to irradiation under continuous stirring at room temperature (25°C) for 180 minutes. At interval of 20 min, aliquot of 5ml was taken and filtered using 0.45 µm cellulose nitrate filter and analyzed for residual concentration of MB at 662nm using a T60 UV-Vis spectrophotometer. The percent photodegradation efficiency (D%) was calculated using Eq. (11).

$$D\% = \frac{[MB]_o - [MB]_t}{[MB]_o} \times 100 \quad (11)$$

Where $[MB]_o$ and $[MB]_t$ is the initial and final concentration of MB, and t is the irradiation time. Thereafter a comparative study such as dark adsorption

and photolysis over the bare ZnO and Cu-doped ZnO catalysts were also determined. These were compared with photocatalysis over Cu-tunable *p*-type ZnO photocatalyst.

2. 6. Controexperiments

A systematic control experiments for the photocatalytic degradation of methylene blue over the undoped ZnO and Cu-tunable *p*-type ZnO nanoparticles under ultraviolet (UV) (96W halogen lamp) irradiation and natural sunlight illumination at optimal reaction conditions (10.00 mg/L of MB initial concentration, 0.30 g/L of catalysts and initial pH of 6.00) were conducted and compared with the photocatalysis of MB using Cu-tunable *p*-type ZnO photocatalyst under visible (300W Xenon lamp emitting at 400 nm) light irradiation. The power intensity of sunlight was measured by using a solarimeter (SL-200-KIMO) every half-hour and found to be 700Wm^{-2} (the experiments were carried out in January 2023). The percentage photodegradation efficiencies were calculated using Eq. (11).

2.7. Radiscavenger Experiments

To investigate the major role of reactive radicals generated during the photocatalytic removal of MB over the Cu-doped ZnO nanoparticles, the main reactive radicals and holes were detected through the radical scavenging experiments. During the photocatalytic process, the holes (h^+), hydroxyl radical (•OH) and superoxide radical ($•O^-_2$) are trapped by adding ammonium oxalate (AO), (h^+ scavenger), *t*-butanol ((•OH scavenger), and *p*-benzoquinone (($•O^-_2$ scavenger) into the reaction solution respectively. Typically, 10.00mg of Cu-ZnO and 10.00mM of radical scavengers were introduced into 10.00mg/L of MB solution, then the suspension was irradiated using the 300W of Xenon lamp emitting at 400nm for the same time. Finally, the MB photodegradation efficiencies were calculated using Eq. (11).

2.8. Face Central Composite Experimental Design

The experimental design and statistical analysis were done using a face central composite design of Response Surface Methodology (RSM) due to its uniqueness in generating a higher-order surface response. An experimental design was carried out at three-level-three-variable face central composite design (FCCD). These independent variables are the initial MB concentration (A), catalyst loading (B) and initial pH (C) operated at three levels (low, central, high) coded -1, 0 and +1 (Table 1). Other variables such as agitation speed, light intensity, oxygen pressure and delivery volume were maintained constant. A total of 20 experiments (N) were performed based on the formula N = 2^n + 2n + 6. Where n is the number of variables. The D% obtained from these experiments were processed using Design Expert software version 12.00 to obtain the predicted responses, response surface and regression model for the MB degradation.

Table 1. Initial experimental levels and codes of variables

Variable	Notation	Levels (Codes)		
Initial MB concentration (mgL^{-1})	A	10 (-1)	20 (0)	30 (+1)
Catalyst loading (gL^{-1})	B	0.1 (-1)	0.3 (0)	0.6 (+1)
Initial pH	C	2 (-1)	6 (0)	10 (+1)

2.9 Kinetic Scheme

To study the kinetic scheme of the MB photocatalytic degradation over the Cu-doped ZnO photocatalyst, experiments were conducted at the optimal operating conditions obtained from the response surface methodology. Similar experiments were performed using the undoped ZnO nanoparticles and compared with that of the Cu-doped ZnO catalyst. The data were fitted into the integrated rate equations (Eqs.12-15) for zero, pseudo-first, second order kinetic reactions and half -life for pseudo-first order model.

$$\frac{[MB]_0}{[MB]_t} = -k\,t \quad (12)$$

$$\ln\frac{[MB]_0}{[MB]_t} = k_{app}\,t \quad (13)$$

$$\frac{1}{[MB]_t} = k\,t + \frac{1}{[MB]_0} \quad (14)$$

and

$$t_{½} = \frac{0.6988}{k} \quad (15)$$

Where $[MB]_0$ and $[MB]_t$ are the initial and final concentration of methylene blue, t is the irradiation time, k and k_{app} are the rate constant and apparent rate constant respectively and $t_{½}$ is the half-life for pseudo-first order reactions. The basic kinetic parameter (*k)* was calculated from the plot of $\frac{[MB]_0}{[MB]_t}$ against t for pseudo-zero order kinetics. Similarly, a plot of $\ln\frac{[MB]_0}{[MB]_t}$ versus t gave a linear graph that passing through the origin and the apparent rate constant, k_{app} (min^{-1}) was estimated from the slope. While the plot of $\frac{1}{[MB]_t}$ against t also gave a linear graph that passing through the intercept in which the MB initial concentration was calculated from intersect and rate constant (k) from the slope. The half-life for the photocatalytic degradation of MB over the synthesized photocatalysts was calculated at optimal conditions.

3. Results and Discussion

3.1. Crystallographic Analysis

The obtained diffraction patterns for the undoped and Cu-doped ZnO photocatalysts are depicted in Fig. 2 (a) and (b) respectively. It can be seen from the Fig. 2 that the diffraction patterns for the undoped and Cu-doped ZnO photocatalysts were consistent with that of the standard ZnO photocatalyst. However, two additional peaks were observed at approximately 2-theta 35° and 39° in Fig. 2b. These peaks indicate the presence of copper which is

consistent with the previous work [65, 66]. Also the intensity of the peaks for the Cu-doped ZnO was decreased when compared with that of the undoped ZnO catalyst. This clearly demonstrated the successful incoporation of the copper onto the surface of bare ZnO nanoparticles.

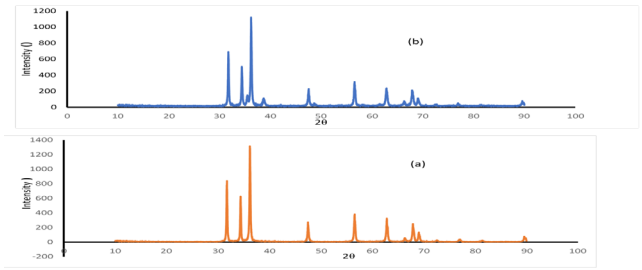

Fig. 2. X-ray diffraction (a) undoped ZnO (b) Cu-doped ZnO photocatalysts

It can be seen from Table 2.**1** that the lattice parameters calculated of bare ZnO are a = b = 0.3235nm and c = 0.5205nm and Cu-doped ZnO are a = b = 0.3261nm and c = 0.5273nm respectively were matched with that of standard hexagonal wurtzite structure of ZnO photocatalyst.

Table 2.1 Calculated lattice parameters for the undoped and Cu-doped ZnO photocatalysts.

Photocatalyst	**a, nm**	**c, nm**	**c/a**	**V, nm^3**	**d. nm**
Undoped ZnO	0.3235	0.5205	1.6089	0.0537	0.0231
Cu-doped ZnO	0.3261	0.5273	1.6169	0.0610	0.0242

The Cu in ZnO is divalent, and the radius of Cu^{2+} (0.073nm), and the radius of the Zn^{2+} (0.074nm) are very close and thus make the change of the lattice constant small and as a result ZnO nanocrystals does not undergo significant lattice distortion.
It is also seen from Table. 3.1, that the average crystallite size (using the high intensity (111) diffraction peak) for the bare ZnO and Cu-tunable p-type ZnO nanoparticles were found to be 29.52nm and 21.95nm respectively, which is consistent with the literature report [60, 61]. These might to be attributed to large surface area of the Cu-ZnO catalyst.

Table 3.1. Physiochemical properties of the undoped and Cu-doped ZnO photocatalyst

Photocatalyst.	**Crystallite size, D (nm)**	**Specific surface area (m^2g^{-1})**	**Band gap (eV)**
Undoped ZnO	29.52	32.42	3.26
Cu-doped ZnO	21.95	48.27	2.99

The specific surface area of the Cu-doped ZnO ($48.27m^2g^{-1}$) (Table. 3) increased compared with that of bare ZnO ($32.42m^2g^{-1}$). This might to be attributed to the reduced particle size and thus doping of copper onto the ZnO nanoparticles would enhance the photocatalytic degradation of methylene blue under visible light irradiation.

3.2. Morphological Analysis.

The scanning electron microscopy (SEM) obtained for the undoped and Cu-doped ZnO photocatalysts are presented in Fig. 3 (a) and (b) respectively. From the Fig. 3(a), formation of homogeneous and uniformly dispersed nanoparticles have been seen. Influence of grain size have been seen and the average particle size also decrease as a result of the copper doping in ZnO matrix (Fig 3 b).

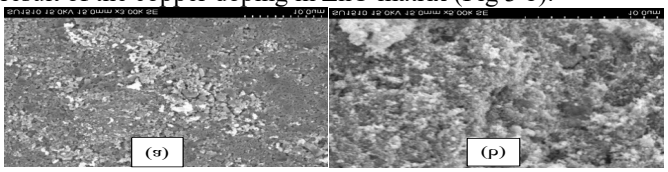

Fig. 3. SEM spectra (a) Undoped ZnO and (b) Cu-doped ZnO photocatalyst

3.3. Optical Analysis

The band gap (E_g) values of the undoped and Cu-doped ZnO photocatalysts obtained are displayed in Fig. 4 (a) and (b) respectively.

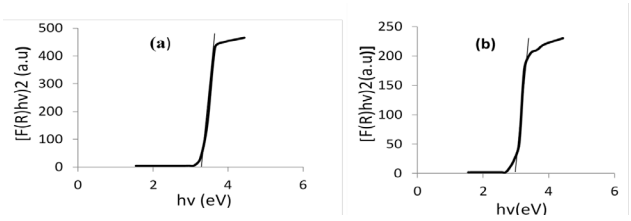

Fig. 4. Tauc's plot (a) Undoped ZnO and (b) Cu-doped ZnO photocatalyst.

This plot is linear in the vicinity of the band gap region for both the Cu-doped ZnO and that of the bare ZnO, revealing that the Cu-doping did not change direct electron transition characteristic of ZnO [67]. The band gap energy values for the undoped and Cu-doped ZnO photocatalysts were 3.26 and 2.99 eV, respectively, confirming the ability of the former to relatively absorb more visible-light. This demonstrated that the Cu-tunable *p*-type ZnO photocatalyst reduces the band gap energy value of the bare ZnO catalyst due to the decreased in the particles size and adsorption capacity between the Cu-doped ZnO nanoparticles and methylene blue which further contributes to the charge-transfer process easily [68, 69, 70]. However, the relatively easier the charge-transitions showed that the Cu-doped ZnO photocatalyst exhibited high electrical conductivity in comparison to the bare ZnO nanoparticles. As a result the Cu-tunable *p*-type ZnO photocatalyst is a good conductor of electricity and can be used as an electrocatalyst during the electrochemical reactions [71, 72].

3.4. Elemental Analysis

Fig. 5 (a) and (b) show the elemental composition of the undoped and Cu-doped ZnO photocatalysts respectively. From the figure 5 (a), only zinc and oxygen atom are present in the EDX spectrum of the undoped ZnO photocatalyst. This confirmed that the synthesized undoped ZnO is a pure zinc oxide. While figure 5 (b) demonstrated the present of copper, zinc and oxygen atom in the EDX spectrum of the Cu- doped ZnO photocatalyst.

This also confirmed the successful doping of Cu on the ZnO nanoparticles.

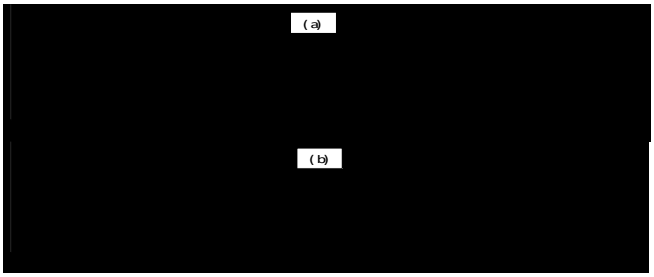

Fig. 5. EDX spectra (a) undoped ZnO (b) Cu-doped ZnO photocatalyst

The weight and atomic percent composition of Zn and O atoms for the undoped and Zn, O and Cu atoms in the Cu-doped ZnO are displayed in Table 4. Even though usually ZnO is considered as an n-type semiconductor where most defects are interstitial zinc and oxygen vacancy, our results showed the deficiency of zinc and excess of oxygen which implies the existence of interstitial oxygen and the less observed p-type semiconducting ZnO nanoparticles.

Table 4: Weight and Atomic percentage of the constituents of undoped and Cu-doped ZnO photocatalyst

Element	**Undoped ZnO**		**Cu-doped ZnO**	
	Wt%	At%	Wt%	At%
CuK	-	1	3.95	2.50
OK	18.79	50.41	23.01	54.87
ZnL	81.21	49.59	73.04	42.63
Total	**100 %**		**100 %**	

3.5. Photocatalytic Activities

3.5.1. Effect of Initial Concentration of MB

To determine the effect of initial concentrations of MB, experiments were performed by varying the initial concentration of MB (5-25mg/L). The amount of the photocatalyst (0.3g/L), initial pH (8) of the suspension, volume of the solution and illumination time were kept constant, and the results obtained was depicted in Fig. 6.

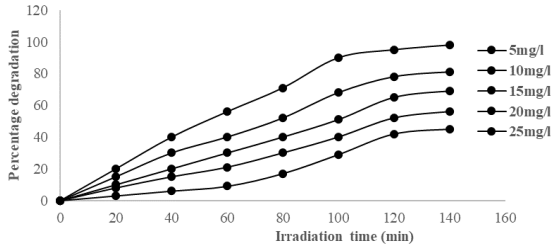

Fig. 6. Effect of initial concentration of methylene blue

It seen from the figure that the percentage degradation efficiency increases with decreasing of the initial concentration of MB. This is because the number of photons absorption by the catalyst increases in the lower concentration regime. This suggest that as the initial concentration of MB increases the requirement of the photocatalyst surface needed for the degradation also increases. Since the illumination time and amount of the photocatalyst are constant, the •OH radical (primary oxidant) formed on the surface of ZnO is also constant. Consequently, the relative number of the free radical attacking the MB molecule decreases with increasing amount of the photocatalyst [73]. While the percentage photodegradation of MB decreases with the increasing of the initial concentration. This is because the number of photons absorption by the photocatalyst decreases in the higher concentration of MB and requirement of the catalyst surface required for the degradation also increases.

3.5.2. Effect of Catalyst Dosage

To determine the optimum amount of catalyst loading in the photocatalytic degradation of MB, various amount of catalyst (0.01-0.06g/L) were used while initial concentration (10mg/L), initial pH (8), volume of solution and illumination time were kept constant. Fig. 7, shows the effect of catalyst loading for the photocatalytic degradation of MB over the Cu-doped ZnO nanoparticles. From the Fig.7, the increase in the amount of Cu-doped ZnO from 0.01 to 0.02g /L slightly increases the percentage degradation of MB due to availability of active sites with increases of catalyst loading.

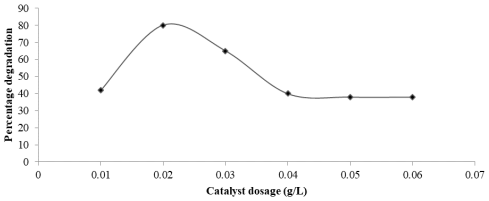

Fig. 7. Effect of catalyst loading

Decline in the degradation efficiency of MB was observed at amount of catalyst above 0.02g/L. Thus 0.02g/L of Cu-doped ZnO photocatalyst was found to be the optimal amount when compared with the rest amount of catalyst. The slight decrease in degradation of MB may be due to the aggregation of Cu-doped ZnO photocatalyst.

3.5.3. Effect of Initial pH

To investigate the effect of initial pH on the photocatalytic degradation of MB over the Cu-doped ZnO photocatalyst, experiments were carried out by varying the initial pH in the range (2-12). In the experiments pH was adjusted by adding appropriate drop of HCl or NH_4OH solution while the initial concentration, catalyst dosage, volume of solution and illumination time were kept constant, and the result was displayed in Fig. 8. From the figure it can be seen that there was a mild increase in degradation with an increase in initial pH.

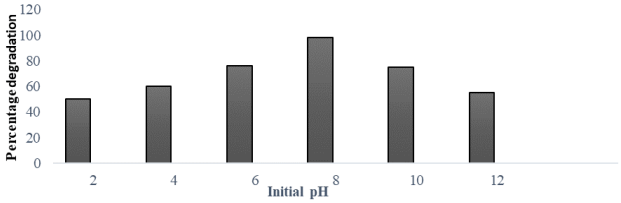

Fig. 8. Effect of initial pH

It is also observed that the percentage removal is higher at initial pH value greater than 2 and less than 10. The solution pH affects the surface charge of Cu-doped ZnO and availability of hydroxyl radicals. At high pH values (greater than 8) the hydroxyl radicals are so rapidly scavenged that they do not have the opportunity to react with MB. The pH affects not only the surface properties of Cu-doped ZnO, but also the dissociation of MB and formation of hydroxyl radicals. Thus, the degradation of MB in this work was more efficient under basic (8) conditions than under acidic conditions. This is because under basic conditions, the •OH radicals are generated more easily by oxidizing more hydroxide ions available the catalyst surface, the efficiency of the process is enhanced. Similarly, at low pH, reduction by electrons in the conducting band may play a very important role in the degradation of MB due to the reductive cleavage of azo bonds.

3.5.4. Photolysis, Adsorption and Photocatalysis under Visible light Irradiation

To determine the photocatalytic activity of the synthesized Cu-tunable *p*-type ZnO photocatalyst for the degradation of MB, an experiments were performed under different conditions such as (1) solution of MB with visible light without the Cu-ZnO catalyst (photolysis), (2) solution of MB with Cu-ZnO catalyst and without the visible light (adsorption), (3) solution of MB with ZnO catalyst and visible light (photocatalysis over the ZnO) and (4) solution of MB with Cu-doped catalyst and visible light (photocatalysis over the Cu-ZnO) and the result was depicted in Fig. 9. From the figure, it seen that the percentage removal (17.23%) of MB obtained under photolysis is not significant after 140 minutes. This shows that light has little effect on the degradation of MB.

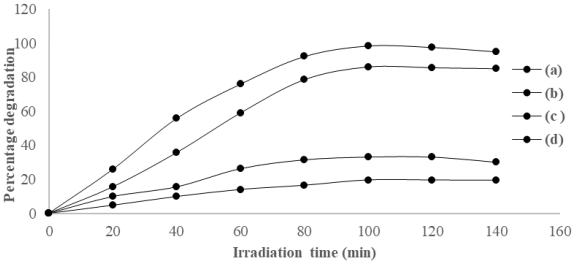

Fig. 9. Effect of irradiation time on the photocatalytic degradation of MB under different processes. (a) Photolysis. (b) Adsorption. (c) Photocatalysis over undoped ZnO. (d) Photocatalysis with Cu-doped ZnO. MB initial 5 mg/L, catalyst dose = 0.02 g/L, and pH =8.

The percentage degradation of MB obtained under adsorption was 23.42%. While the percentage efficiency for the degradation of MB over the undoped ZnO and Cu-doped ZnO photocatalysts under visible light after 140minutes are 81.76 and 98.96% respectively. This clearly, indicates that light and catalyst are necessary for the effective photocatalysis. However, the photacatalytic activity of Cu tunable *p*-type ZnO is higher than that of the bare ZnO under visible light due its lower band gap energy (2.99eV) and slow rate of electron recombination process.

3.5.5 Photocatalysis under Ultraviolet (UV) Irradiation

Fig. 10 shows the effect of irradiation time on the photocatalytic degradation of MB over the bare ZnO and Cu-tunable *p*-type ZnO nanoparticles under ultraviolet light irradiation at 140 min.

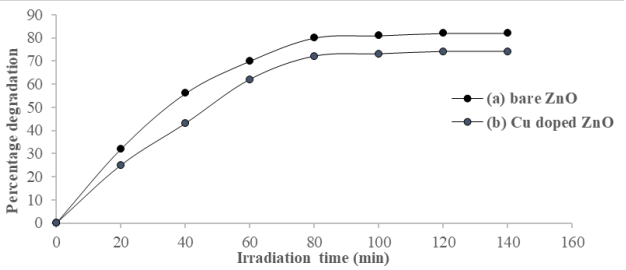

Fig. 10. Effect of irradiation time on the photocatalytic degradation of MB under UV light irradiation (a) over bare ZnO nanoparticles (b) over Cu-tunable *p*-type ZnO nanoparticles

From the Fig.10, the percentage removal of MB by photocatalysis over the bare ZnO and Cu tunable *p*-type ZnO nanoparticles were found to be 81 % and 70 %, respectively, which clearly demonstrates that the as-synthesized ZnO photocatalyst has a better photoeffiencies for the removal of MB than the Cu-doped ZnO catalyst under this condition. The high photocatalytic activity of the ZnO NPs can be attributed to the possible penetration and high stimulation of nanoparticles by ultraviolet (UV) lamps. This however supports the results of Ahmad *et al.* [59] under ultraviolet light irradiation, which revealed that bare ZnO is more active than Cu- tunable ZnO nanoparticles under UV irradiation [62].

3.5.6 Photocatalysis under Natural Sunlight Irradiation

Fig. 11 shows the effect of irradiation time on the photocatalytic degradationof MB over the bare ZnO and Cu-doped ZnO nanoparticles under natural sunlight irradiation at 140 min.

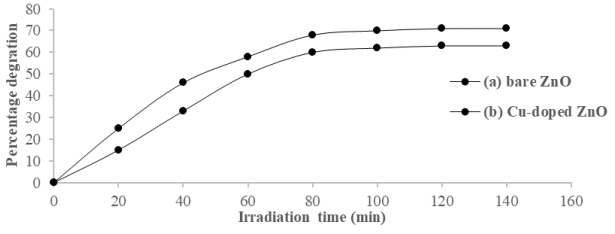

Fig. 11. Effect of irradiation time on the photocatalytic degradation of MB under sunlight irradiation (a) over bare ZnO nanoparticles (b) over Cu-tunable ZnO nanoparticles

Conversely, the Fig. 11 indicated that the percentage removal of MB by photocatalysis over the undoped ZnO and Cu-doped ZnO nanoparticles were 69 % and 58 %, respectively, which clearly demonstrates that the as-synthesized bare ZnO photocatalyst has a better photoeffiency for the removal of MB than the Cu-doped ZnO catalyst. The high photocatalytic activity of the undoped ZnO can be attributed to the possible penetration and high stimulation of nanoparticles by sunlight. This however supports the results of Nouasria *et al.* [61] under sunlight, which revealed that the bare ZnO is more active than Cu doped ZnO nanoparticles. Based on these findings the photocatalytic degradation of MB over the undoped and Cu-doped ZnO nanoparticles under the visible light irradiation exhibited the higher photocatalytic activity (82% and 96 %) in comparison to the results obtained under the UV irradiation (81 % and 70 %) and natural sunlight (69 % and 58 %) for the bare ZnO and Cu-doped ZnO nanoparticles respectively. Therefore, visible light is more economical, enhanced photocatalytic performance and generate less operational problem during heterogeneous photocatalysis [74].

Furthermore, the spectral results obtained from the XRD and UV/Vis spectrophotometry of the as-synthesized Cu-tunable *p*-type ZnO nanoparticles clearly demonstrates that the specific surface area has increased in comparison to the bare ZnO nanoparticles. The increased in the surface area of the as synthesized Cu-doped ZnO photocatalyst has been related to enhance the interfacial photoreactions between the Cu- ZnO catalyst and the MB. Similarly, the band gap energy for the Cu-doped ZnO catalyst has been reduced (2.99 eV) in comparison to the bare ZnO nanoparticles (3.26 eV). Accordingly, the lower the value of the band gap energy the greater the possibility to enhance the photocatalytic reactions. Conversely, the experimental results observed from the series of experiments on the photocatalytic degradation of MB over the Cu-doped ZnO nanoparticles under visible light irradiation beautifully revealed the significant percentage degradation efficiency due to its increase in surface area (48.27 m^2g^{-1}) and lower band gap energy value (2.99 eV) when compared with that of the bare ZnO catalyst with surface area (32.42 m^2g^{-1}) and band gap energy value (3.26 eV). In comparison, the spectral results of the as synthesized ZnO nanoparticles harvested from the spectral analyses were in good agreement with the experiment results observed on the photocatalytic removal of methylene blue over the photo responsive Cu tunable *p*-type ZnO nanoparticles.

3.6 Mechanism of Photocatalytic Degradation of MB

The mechanism of photocatalysis generally involves the photoexcitation, separation, migration of charge and redox reactions on the surface of the photocatalyst [75]. The reactive species generated during illumination of photocatalysts are hole (h^+), hydroxyl radical (•OH) and superoxide ($•O_2$). A typical mechanism for the photocatalytic degradation of MB over (a) the bare ZnO under UV irradiation (b) the Cu tunable *p*-type ZnO nanoparticles under visible light irradiation is shown in Fig. 12.

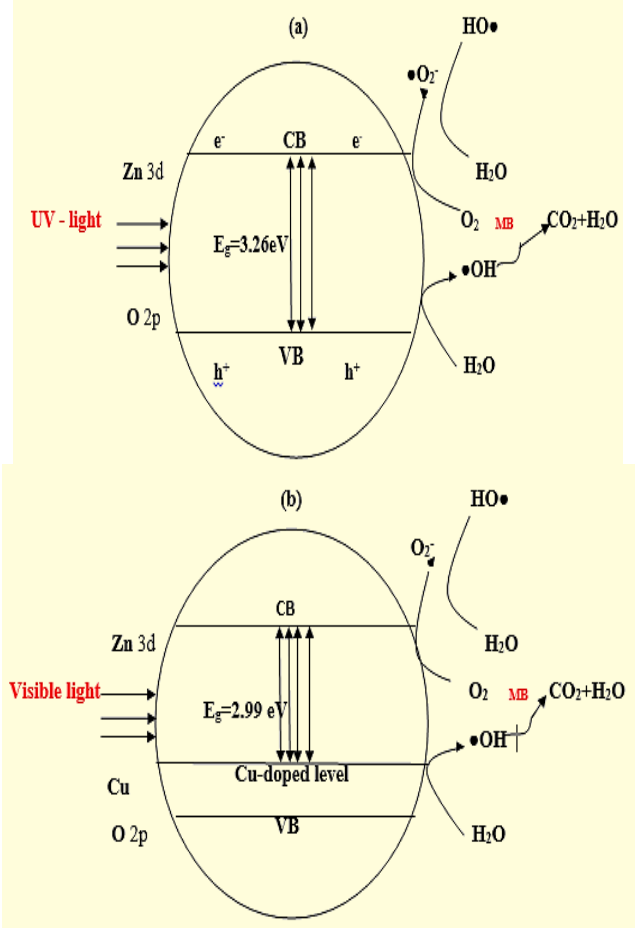

Fig.12. Mechanism of photodegradation of MB (a) over ZnO nanoparticles under UV irradiation (b) over Cu tunable *p*-type ZnO nanoparticles under visible light irradiation

However, in a typical process of photocatalysis, the electrons in valence band (VB) transfer to the conduction band (CB) under UV/Visible irradiation of the photocatalyst. The corresponding energy is higher than the band gap of the ZnO (3.26/2.99 eV) there by promoting the generation of conduction band electrons and valence band holes. The photogenerated holes could either directly oxidize adsorbed MB or react with hydroxyl or water to generate hydroxyl radical. Similarly, the photoelectrons reduce oxygen adsorbed on the photocatalyst surface into superoxide radical. Finally, MB was decomposed by generated hydroxyl and superoxide radical into environmentally friendly species and mineral salts according to the equations 16, 117, 18 and 19.

$$Cu - ZnO + h\vartheta \rightarrow h^+ + e^- \quad (16)$$

$$h^+ + OH^- \text{ or } H_2O \rightarrow • OH \quad (17)$$

$$e^- + O_2 \rightarrow • O_2^- \quad (18)$$

$\bullet OH/\bullet O_2^-$ + MB → CO_2 + H_2O + mineralized (19)

The tunable of copper onto the ZnO lattice leads to the formation of a new mid gap energy state (Fig. 12. b), that is the Cu band above the O valence band, which eventually decreases the band gap of ZnO and shifts the optical absorption to the visible light regions.

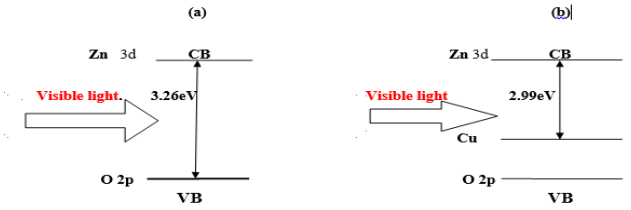

Fig. 13. Energy level diagram (a) bare ZnO (b) Cu-tunable *p*-type ZnO photocatalyst.

Fig. 13 represents the band gap state for the unmodified and modified ZnO nanoparticles. From the Fig. 13 (b), it is possible for the electrons to migrate from the valence band to the conduction band of the modified photocatalyst and thus, absorbing visible light irradiation in the photocatalytic degradation reaction which leads to visible light activity of Cu tunable *p*-typed ZnO catalyst. The Fig.13 (b) further, shows the generation of electron in the conduction band and holes in the valence band under visible light illumination, these electrons in the conduction band accumulate on the catalyst surface and are then scavenged by oxygen molecule, either the presence of copper can alter the band structure or suppress the recombination efficiency of the photo-generate electron-hole pairs, resulting in an enhanced photocatalytic capacity of ZnO in the visible light region [74]

However, to explain extensively the mechanism of Cu tunable p-type ZnO nanoparticles for the degradation of methylene blue, it is very essential to find out which reactive free radicals contributes immensely in the photocatalytic degradation reaction. In the photocatalytic reaction of MB over Cu tunable ZnO nanoparticles, the h^+, • OH, and $\bullet O_2^-$ are generated by adding AO (h^+ scavenger) [76], *t*-BuOH (• OH scavenger) [77] and *p*-BQ ($\bullet O_2^-$ scavenger) [78] into the reaction solution respectively and the result is depicted in Fig 14.

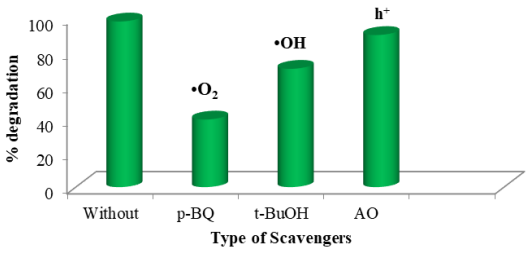

Fig 14. Degradation efficiency of MB in the absence and presence of scavengers

Fig 14 demonstrates that the addition of *t*-BuOH and AO only slightly changed in the photocatalytic degradation of MB was obtained while the addition of *p*-BQ scavenger significantly changed was observed. These indicate that the decrease of the photocatalytic degradation in the presence of scavengers present the following trends: benzo-quinonine > tertiary-butanol > ammonium oxolate, which is very similar to the results of Huang *et al* [79]. Hence, the superoxide radicals are the mains reactive species during the photocatalytic degradation of MB under visible light irradiation.

3.7 Optimization Section

The experimental and predicted degradation efficiency obtained are shown in Table 5. The predicted degradation (D_{cal} %) fit the generic, second order polynomial model in eq. (20). The experimental optimum degradation efficiency (98%) was achieved at A = 10.00 mgL^{-1}, B = 0.3gL^{-1} and C = 6.

$$D\% = +80.73+1.28A-1.98B+0.98C+2.22A^2+0.20B^2+0.98C^2 +0.70AB+1.50AC+2.80BC \quad (20)$$

Table 5. Results of FCCD with experimental and predicted values.

Run	Variables			Degradation efficiency (%)	
	A	B	C		
	(experimental)		(predicted)		
1	10	0.1	10	87.27	88.92
2	10	0.6	2	85.21	87.07
3	30	0.6	10	85.68	77.95
4	20	0.3	6	76.88	78.92
5	20	0.6	10	81.27	82.15
6	20	0.6	6	75.66	86.31
7	10	0.6	10	81.33	82.39
8	30	0.1	2	88.09	89.36
9	20	0.3	6	80.99	84.86
10	20	0.3	6	97.18	89.18
11	20	0.3	6	92.18	84.64
12	10	0.1	2	74.57	77.98
13	20	0.3	2	79.24	81.95
14	20	0.3	6	91.88	85.04
15	20	0.1	6	77.18	80.73
16	30	0.6	2	90.65	80.73
17	30	0.1	10	70.65	80.73
18	30	0.3	6	86.11	80.73
19	10	0.3	6	98.09	97.73
20	20	0.3	6	80.20	80.73

However, the closeness of the values between the experimental and predicted response is a clear indication of the accuracy of the model. Similarly, this good correlation is attested the linear normal plot of residual (Fig. 15). Majority of the points on the normal probability plot lies roughly on a straight line, so it can conclude that

the estimated effects are real and differ markedly from noise.

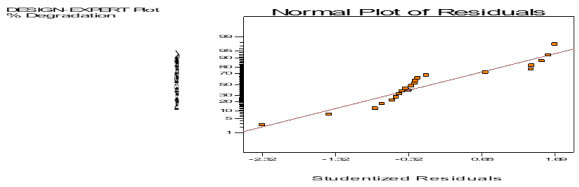

Fig. 15. Linear normal plot of residual

Analysis of variance (ANOVA) was performed in order to check the model accurately by evaluating the sum of squares, degree of freedom, mean square, F-value and p-value and the results are shown in Table 6. From the Table, the model-value of 11.88 implies model significance and that there is only a 0.03 % chance of a noisy model F-value. The quality of the developed model is high given that R^2 = 0.9815. This implies that 98 % of the variations for the degradation of MB dye were explained by the independent variables within the studied range. The lack of fit value of 0.49 is not significant relative to the pure error when p-value is 0.6562 (more than 0.05) which shows good predictability of the model. Meanwhile, the significance of the model terms is proven by the small p-value (less than 0.0001). Therefore, the significant terms among the tested process parameters were solution pH > MB concentration > second order of solution pH > second order of Cu-ZnO photocatalyst dosage > Cu-ZnO photocalyst dosage > second order of MB concentration. Other model terms are insignificant as their p-value were greater than 0.1000.

From the table 7, the coefficient of variance (C.V. = 1.24) is low indicated high precision and good reliability of the experimental values. Adequate precision measure of 31.47, which is well above 4 indicates an adequate signal. The regression model demonstrates a good relationship between independent variables, as both R^2 (0.9786) was close to 1. In the study, the p-values of the major parameters (A and C) influencing the percentage removal of MB are significant (P<0.05). Similarly, the interaction terms (AC) as well as the quadratic terms (A^2) have probabilities less 0.05, which indicates they significantly contribute to the degradation of MB.

Table 6: ANOVA for response surface quadratic model.

Source	Sum of Square	DF	Mean Square	F-value	P-value	Remarks
Model	257.99	9	28.00	11.8844	0.0004	significance
A	22.47	1	22.47	81.43	<0.0001	
B	53.56	1	53.56	8.77	0.0145	
C	11.57	1	11.57	7.90	0.0125	
A^2	71.21	1	71.21	1.12	0.03131	
B^2	0.60	1	0.60	9.412E-003	0.9245	
C^2	13.74	1	13.74	0.22	0.6523	
AB	3.96	1	3.96	0.062	0.8082	
AC	18.03	1	18.03	0.28	0.6064	
BC	62.78	1	62.78	0.98	0.3444	
Residual	637.40	10	637.40			
Lack of fit	388.88	5	77.78	0.49	0.6562	not significant
Pure Error	248.52	5	49.70			
Cor. Total	889.40	19				

Table 7. Analysis of variance (ANOVA) results for the response quadratic model

Parameter	Value
Standard deviation	2.01
Mean	88.94
Coefficient of variance (CV,%)	1.24
Coefficient of determination (R^2)	0.9768
Adjusted R^2	0.9595
Predicted R^2	0.7889
Adequate precision	31.47

To validate the quadratic model obtained in this study, runs were individually performed and compared to the predicted results (Table 8). The experimental results were very close to the predicted values (98.46 %) confirming the reliability of the FCCD.

Table 8. Validation data of the quadratic model.

Run	Initial MB concentration (mg/L)	Catalyst loading (gL^{-1})	Initial pH	Experimental efficiency (%)	Predicted efficiency (%)
1	10.00	0.3	6.00	98.46 ± 0.10	98.01
2	20.00	0.1	8.00	77.99 ±0.21	76.80
3	20.00	0.6	10.00	71.69± 0.45	71.34

Fig.16 (a) shows a three-dimensional response surface and contour plot of the influence Cu-doped ZnO catalyst and initial MB concentration at constant initial pH. It is evident that the removal percentage increased proportionally with increase of photocatalyst dosage due to enhancement in the generation of hydroxyl radicals. Higher catalyst loading was antagonistic to the degradation process, perhaps due to reduction in catalyst surface area available for light absorption and MB adsorption. On the other hand, the interaction effect of Cu-doped ZnO loading and initial pH of reaction mixture on the degradation of MB dye is depicted in Fig. 16 (b). From the response surface and contour plot, the degradation efficiency was low at acidic pH value due to the loss of Cu-doped ZnO perhaps, whereas at alkaline medium hydroxyl radicals played a positive role in the removal of MB as earlier observed in the case of other organic contaminants. Lastly, Fig 16(c) shows the effect of MB initial concentration and initial solution of pH in removing MB dye. However, the degradation efficiency reduced with increasing MB concentration ascribed to the interception of photon before

they reach the surface of the Cu-ZnO photocatalyst. Moreover, the columbic repulsion between the negatively charged Cu-doped ZnO photocatalyst surface and hydroxyl anions at highly alkaline condition reduced the MB removal rate via suppression of the generation of hydroxyl radicals.

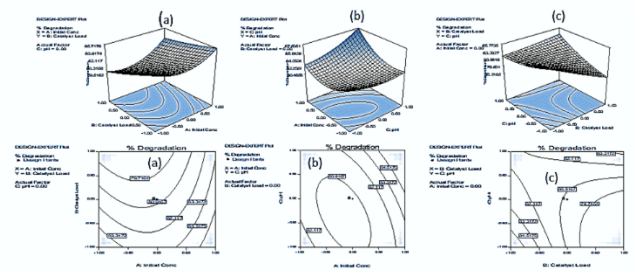

Fig. 16. The 3D response surfaces and contour plot for a (a) initial concentration and catalyst dosage (b) initial concentration and initial pH (c) catalyst dosage and the initial pH

3.8. Reusability and Stability Test

In order to determine the reusability of the Cu-doped ZnO photocatalyst systematic experiments were performed at the optimum conditions of the photocatalytic degradation of MB over the Cu-doped ZnO. Residual catalyst from degradation experiment was filtered, washed and dried and then recycled in fresh experiment and the result was illustrated in Fig. 17.

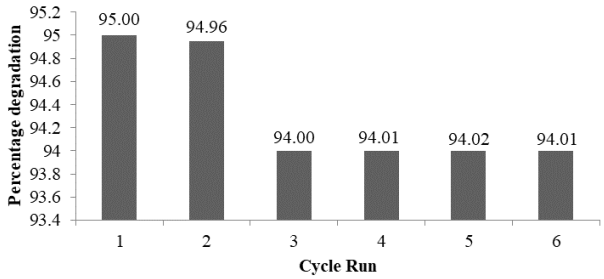

Fig. 17. Reusability of Cu-tunable ZnO in degradation of MB.

From the Fig.17, it can be seen that the degradation of methylene blue decreased steadily from the 1st and 2nd cycles, but 3rd, 4th, 5th and 6th cycles remained the same. This clearly shows the stability and effectiveness of the Cu-doped ZnO photocatalyst in the degradation of methylene blue.

3.9. Kinetics Section

The effects of the photocatalytic degradation of MB over the bare ZnO photocatalyst were studied and compared with the photocatalytic removal profiles over the Cu-doped ZnO photocatalysis. The results are depicted in Fig. 18. It can be observed from the Fig.18 that the plot of $\ln\frac{[M]_0}{[M]_t}$ verse time gives a straight-line graph that passing through the origin for both undoped and Cu-doped ZnO. Therefore, the photocatalytic removal of MB over the ZnO and Cu-doped ZnO nanoparticles were nicely fitted pseudo-first order model when compared with the pseudo-zero and pseudo-second order plots.

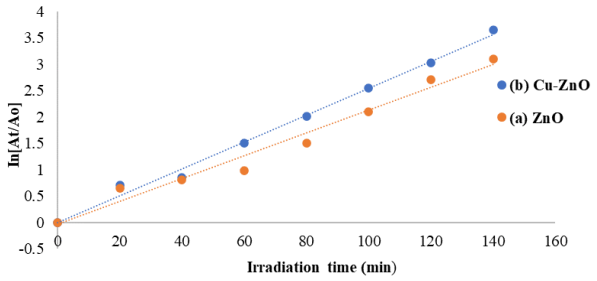

Fig. 18. Pseudo-first order plot (a) over bare ZnO (b) over Cu-doped ZnO catalyst

The rate constant corresponding each equation was obtained from the slope. The rate constant (k) and half-life ($t_{½}$) obtained in this study is presented by the Table 9. The photocatalytic degradation of methylene blue over the bare ZnO and Cu-doped agreed with the pseudo-first order kinetic scheme with rate constant (k) of 1.6 x 10^{-3} min^{-1} and 1.8 x 10^{-3} min^{-1} respectively.

Table 9. Kinetic parameters for bare ZnO and Cu-doped ZnO photocatalyst

Catalyst	Pseudo-zero-order			Pseudo-first order			Pseud-second order		
	k(10^{-3} $moldm^{-3}s^{-1}$)	R^2	$t_{½}$	k(10^{-3} min^{-1})	R^2	$t_{½}$	k (10^{-3} $moldm^{-3}s^{-1}$)	R^2	$t_{½}$
Bare ZnO	1.32	0.956	2.87	1.60	0.973	3.23	1.11	0.894	1.37
Cu- ZnO	1.35	0.958	2.97	1.87	0.98	4.86	1.15	0.898	1.90

4. Conclusion

The visible light photo responsive Cu-tunable *p*-type ZnO photocatalyst with relatively reduced particle size, band gap energy, and increased surface area was successfully synthesized by a sequential co-precipitation method. Doping with copper tuned up the photocatalytic activity of the ZnO and reduced the rate of electron recombination process. In the study the spectral results were consistent with experimental results. The superoxide radicals is the main reactive species during the photocatalytic degradation of MB under visible light irradiation. The optimum degradation efficiency for the photocatalytic degradation of MB over the Cu tunable *p*-type ZnO was found to be 98.00% at 10mg/L initial concentration of MB, 0.30g/L catalyst dosage and initial solution pH at 6.00. The kinetics for the MB removal was proceeded in a pseudo-first order kinetic scheme with peak rate constant of 0.0016 min^{-1} and 0.0018 min^{-1} for the bare and Cu tunable *p*-type ZnO nanoparticles respectively.

Acknowledgement
The authors are very grateful to the Department of Applied Chemistry, Faculty of Physical Sciences, Federal University Dutsin-Ma, Katsina state, Nigeria for providing most of the facilities required for this research work.

References

[1] V. I. Parvulescus, F. Epron, H. Garcia and P. Grangers, Recent Progress and Prospect in Catalytic Water Treatment: *Chemical Reviews*, 2021, 122, 101-112.
[2] V. K. Gupta, I. Ali, T. A. Saleh, A. Nayak and S. Agarwal, Chemical Treatment Technologies for Waste-water Recycling, An Overview: *RSC Advance*, 2012, 2 (16), 6380
[3] P. Rajasulochana and V. Preethy, Comparison on Efficiency of Various Techniques in Treatment of Waste and Sewage water-a Comprehensive Review: *Resource Efficient Technologies,* 2016, 2(4), 175-184.
[4] A. Kadam, R. Dhabbe, A. Gophane, T. Sathe and K.Garadkar, Template Free Synthesis of ZnO/Ag_2O Nanocomposites as a Highly Efficient Visible Active Photocatalyst for Detoxification of Methyl Orange: *Journal of Photochemistry and Photobiology*, 2016, 154, 24-33.
[5] G. Yang, D. Zhang, G. Zhu, A Sm- MOF/GO Nanocomposite Membrane for Efficient Organic Dye Removal from Wastewater: *RSC Advance*, 2020, 10 (14), 8540-8547.
[6] M. T. Amin, A. A. Alazba and U. Manzoor, A Review of Removal of Pollutants from Water/Wastewater Using Different Types of Nanomaterials: *Advances in Materials Science and Engineering,* 2014, ID 825910, 24.
[7] V. A. Escobar-Barrios, D. V.S. Rodrigueez, N. A. C. Rincon and A. B. J. Salcedo, Modified Metallic Oxide for Efficient Photocatalysis, *Photocatalysts-Applications and Attributes, Books on Demand, Nor dersted, Germany*, 2019.
[8] K.A. Isai and V.S. Shrivastava, Photocatalytic Degradation of Methylene Blue using ZnO and 2% Fe-ZnO Semiconductor Nanoparticles Synthesized by Sol-gel Method: A Comparative Study, *SN Appl. Sci*, 2019, 1, 10, 1-11.
[9] A.G. Acedo-Mendoza, A. Infantes-Molina, D. Vargas-Hernandez, C.A Chavez-Sanchez, E. Rodrigues-Castellon, and J.C Tanori-Cordova, Photodegradation of Methylene Blue and Methyl Orange with CuO Supported on ZnO Photocatalysts: The Effect of Copper Loading and Reaction Temperature, *Mater. Sci. Semicond. Process,* 2021, 119, 10527-10530.
[10] A. Dana and S. Sheibani, CNT S-Copper Oxide Nanocomposite Photocatalyst with High Visible Light Degradation Efficiency, *Adv.Powder Technol,* 2021, 10, 32, 3760-3769.
[11] M. Khaksir, M. Amini, and D.M. Bogheei, Efficient and Green Oxidation Degradation of Methylene Blue using Mn-doped ZnO Nanoparticles (Zn1-xMnxO), *Exp. Nanosci*, 2015, 10, 16, 1256-1268.
[12] J. Zhang, Synergistic Effect of Photocatalysis and Thermocatalysis for Selective Oxidation of Aromatic Alcohol to Aromatic Aldehydes using Zn3In2S@ZnO Composite, *Appl. Catal. B Environ*, 2017, 218, 420-429.
[13] N. Soltani, Visible Light-Induced Degradation of Methylene Blue in the Presence of Photocatalytic ZnS and CdS Nanoparticles, *Int. J. Mol. Sci,* 2012, 13, 12242-12258.
[14] T. Ahmed, M. Naushad, G.E. Eldesoky et al., Effective and Fast Adsorptive Removal of Toxic Cationic Dye (MB) from Aqueous Medium using Amino-Functionalized Magnetic Multiwall Carbon Nanotubes, *Journal of Molecular Liquids*, 2019, 282, 154-161.
[15] K. V. Karthik, A.V. Raghu, K. R. Reddy et al., Green Synthesis of Cu-doped ZnO Nanoparticles and its Application for the Photocatalytic Degradation of Hazardous Organic Pollutants, *Chemosphere,* 2022, 287
[16] H. R. Mardani, M. Farunzani, M. Ziari and P. Biparva, Visible Light Photo-degradation of Methylene Blue over Fe or Cu Promoted ZnO Nanoparticles, *Spectrochimica Acta Part A: Molecular and Biomolecular Spectroscopy*, 2015, 141, 27-33.
[17] S. G. Aragaw, F. K. Sabir, D. M. Andoshe, and O. A. Zelekew, Green Synthesis of p-$Co3O_4$/n-ZnO Composite Catalyst with *Eichhornia crassipes* Plant Extract Mediated for Methylene Blue Degradation under Visible Light Irradiation, *Materials Research Express*, 2020, 7(9), Articles ID 095508.
[18] R. Uma, K. Ravichandran, S. Sriram and B. Shakthivel, Cost-Effective Fabrication of ZnO/g-C_3N_4 Composite Thin Films for Enhanced Photocatalytic Activity against three Different Dyes (MB, MG and RhB), *Mater. Chem. Phys,* 2017, 201, 147-155.
[19] Y. K. Manea, A. M. Khan. Enhanced Photocatalytic Degradation of Methylene blue and Adsorption of Metal Ions by SDS-TiP Nano composite*, Journal of Research Articles SN Appied Science*, 2019, 1, 821.
[20] X. Chen, H. Sun, J. Zhang et al., Synthesis of Visible Light Responsive Iodine Doped Mesoporous TiO2 by using Biological Renewable Lignin as Template for Degradation of Toxic Organic Pollutants (MB), *Applied Catalysis B: Environmental*, 2019, 252, 152-163.
[21] M. Irani, T. Mohammadi and S. Mohebbi, Photocatalytic Degradation of Methylene Blue with ZnO Nanoparticles: A Joint Experimental and Theoretical Study, *J. Mex. Chem. Soc,* 2016, 60(4), 218-225.
[22] S. Shankar, M. Saroja, M. Venkatachalam, G. Parthasarathy, Photocatalytic Degradation of Methylene Blue Dye using ZnO Thin Films, *International Journal of Chemistry. Concepts,* 2017, 3, 180-188.
[23] W. Vallejo, A. Cantillo, B. Salazar, C. Diaz-Uribe, W. Ramos, E. Romero, M. Hurtado, Comparative Study of ZnO Thin Films Doped with Transition Metals (Cu and Co) for Methylene Blue Photodegradation under Visible Irradiation, *Catalyst*, 2020, 10, 528.
[24] M. Khadaic, N. Ghasemi, B. Moradi and M. Rahimi, Removal of Methylene Blue from Wastewater by Adsorption onto ZnCl2 Activated Corn Husk Carbon Equilibrium Studies: *Journal Chemistry*, 2013, 10, 383985.
[25] Y. N. Teixeira, F. J. P. Filho, V. P. Bacurau, J. M. C. Menezes, A. Z. Fan, R. P. F. Melo, Removal of Methylene Blue from a Synthetic Effluent by Ionic Flocculation: *Heliyon*, 2022, 8(10); e10868.
[26] H. Eslami, S. S. Khavidak, F. Salehi, R. Khosravi, R. Fallahzadeh, R. Peirovi and S. Sadeghi, Biodegradation of Methylene Blue from Aqueous Solution by Bacteria Isolated from Contaminated Soil: *Journal of Advance Environmental Health Research*, 2017, 5, 10-15.
[27] S. Moharramzaheh and M. Baghdadi, In Situ Sludge Magnetic Impregnation (ISSMI) as an Efficient Technology for Enhancement of Sludge Sedimentation: Removal of Methylene Blue Using Nitrate Acid Treated Graphene Oxide as a Test Process: *Journal of Environmental Chemical Engineering,* 2016, 4 (2); 2090-2102.

[28] N. H. Thang, D. S. Khang, T. D Hai, D. T. Nga, and P. D. Tuan, Methylene Blue Adsorption Mechanism of Activated Carbon Synthesized from Cashew Nut Shells: *RSC Advance*, 2021, 11, 26563.
[29] Y. Kuang, X. Zhang, and S. Zhou, Adsorption of Methylene Blue in Water onto Activated Carbon by Surfactant Modification: *Water*, 2022, 12, 587.
[30] Z. Derakhshan, M. A. Baghapour, Ranjbar, M. Faramarzian, Adsorption of Methylene Blue Dye from Aqueous Solution Modified Pumice Stone: Kinetics and Equilibrium Studies, *Health Scope*, 2013, 2(3), 136-44.
[31] G. D. C. Tovar, M. Contreras, W. Vallego, C. C. Lopez, Bio-removal of Methylene Blue from Aqueous Solution by Galactomyces Geotrichum KL20, *Wate*r, 2019, 11, 282-13.
[32] I. M. F. Cardoso, R. M. F. Cardoso, J. G. Esteves da Silva, Advanced Oxidation Processes Coupled with Nanomaterials for Water Treatment, *Nanomaterials* 11, 2021, 82045.
[33] E. M. Cuerda-Correa, M. F. Alexandre-Franco, C. Fernandez-Gonazalez, Advanced Oxidation Processes for the Removal of Antibiotics from Water, An Overview, *Water,* 2020, 12, 102.
[34] M. Z. B. Mukhlish, F. Najnin, M. M. Rahman, M. J. Uddin, Photocatalytic Degradation of Different Dyes using TiO2 with High Surface Area: A Kinetics Study: *Journal of Scientific Research*, 2013, 5(2), 301-314.
[35] M. M. Rashid, A. A. Ismail, I. Osama, I. A. Ibrahim, A. T. Kandil, Photocatalytic Decomposition of Dyes Using ZnO doped SnO_2 Nanoparticles by Solvothermal Method: *Arabian Journal of Chemistry*, 2014, 7, 71-77.
[36] D. P. D. Gupta, A. H. Almuhtaseb, G. Sharma, A. Kumar, M. Naushad, T. A. Saad, M. Alshehri, Photocatalytic Degradation of Highly Toxic Dyes Using Chitoson-g-poly (acrylamide) over ZnS in the Presence of Solar Irradiation: *Journal of Photochemistry and Photobiology A*: Chemistry, 2016, 329, 61-68.
[37] E. Repo, S. Rengaraj, S. Pulkka, E. Castangnola, S. Suihkenen, M. Sopanen, and M, Sillanpaa, Photocatalytic Degradation of Dyes by CdS Microspheres Under Near UV-and Blue LED Radiation: *RSC Advance*, 2013, 120, 206-214.
[38] M.B. Tahir, M. Sagir, A. Ahmed, WO_3 Nanostructure Based Photocatalyst Approach Towards Degradation of Rhodamine B Dye: *Journal of Inorganic and Organometallic Polymers and Materials*, 2018, 28, 1107-1113.
[39] N. Elamin and A. Elsanousi, Synthesis of ZnO Nanostructures and their Photocatalytic Activities, *Journal of Applied and Industrial Sciences*, 2013, 1, 32-35.
[40] S. S. Momeni, M. Nasrollahzadeh, and A. Rustaiyan, Green Synthesis of the Cu-doped ZnO Nanoparticles Mediated by Eu Phobia prolifera, Leaf Extract and Investigation of their Catalytic Activity. *Journal of Colloid and Interface Science*, 2016, 472, 173-179.
[41] S. A. Khan, F. Noreen, S. Kanwal, A. Iqbal, and G. Hussain, Green Synthesis of ZnO and Cu-doped ZnO Nanoparticles from Leaf Extract of Abutilon indicum Clerodendrum infortunatum, Clerodendrum inerme and Investigation of their Biological and Photocatalytic Activities: *Material Science and Engineering: C,* 2018, 82, 46-59.
[42] R. Ullah, and J. Duttah, Photocatalytic Degradation of Organic Dyes with Mn-doped ZnO Nanoparticles: *Journal of Hazardous Materials*, 2008, 156, 194-200.
[43] R. E. Adam, H. Alnoor, G. Pozina, X. Liu, M. Willander, and O. Nur, Synthesis of Mg-doped ZnO NPs Via a Chemical Low-Temperature Method and Investigation of the Efficient Photocatalytic Activity for the Degradation of Dyes Under Solar Light: *Solid State Sciences*, 2020, 99, 106053.
[44] A. P.C. Olla, G. Reekman, A. S. Kelchtermans, D. D. Sloovere, et al., Photocatalytic Performance of Undoped and Al-doped ZnO Nanoparticles in the Degradation of Rhodamine B Under UV-Visible Light: The Role of Defect and Morphology*: International Journal of Molecular Sciences*, 2022, 23, 15459.
[45] X. Li, Z. Hu, J. Liu, D. L. Xiao, V. Zhang, and J. C. J. Jialin, Ga-doped ZnO Photonic Crystals with Enhanced Photocatalytic Activity and its Reaction Mechanism: *Applied Catalysis B: Environmental*, 2016, 195, 29-38.
[46] K. A. Isai and V. S. Shrivastava, Photocatalytic Degradation of Methylene Blue Using ZnO and 2% Fe-doped ZnO: *SN Applied Science*, 2019, 1, 1247.
[47] T. M. Elmorsi, M. H. Elsayed. and M. F. Bakir, Na-doped ZnO Nanoparticles Assisted Photocatalytic of Congo Red Dye Using Solar Light: *American Journal of Chemistry*, 2017 7(2); 48-57.
[48] A. Chauhan, R. Verma, R. Kumar, A. Sharma, P. Shandilija, X. Li, K. M. Batoo, A. Imran, S. Kulshrestha, and R. Kumar, Photocatalytic Dye Degradation and Antimicrobial Activiies of Pure and Ag-doped ZnO Using Cannobis Sativa Leaf Extract: *Rep 10*, 2020, 10, 7881.
[49] F. Naz, and K. Saeed, Investigation of Photocatalytic Behaviour of Undoped and Cr-doped ZnO Nanoparticles for the Degradation of Dye. *Inorganic and Nano-Metal Chemistry*, 2021, 51(1); 1-11.
[50] S. Wongrerkdee, S. Wongrerkdee, C. Boonrung, and S. Sujinnaparani, Enhanced Photocatalytic Degradation of Methylene Blue Using Ti-doped ZnO Nanoparticles Synthesized by Rapid Combustion: *Toxic*, 2023, 11(1); 33.
[51] T. M. Elmorsi, Towards Visible-Light Responsive Photocatalysts: Nano-potassium Doping Zinc Oxide (K-ZnO) for Degradation of 2-Naphthol: *Physical Chemistry*, 2017, 7(2); 42-53.
[52] P. Jongnavakit, P. Amoonpitoksuk, S. Suwanboon, and N. J. Ndiege, Preparation and Photocatalytic Activity of Cu-doped ZnO Thin Films Prepared by the Sol-gel Method, *Applied Surface Science*, 2012, 258, 8192-8198.
[53] M. Fu, Y. Li, P. Lu, J. Liu, and F. Dong, Sol-gel Synthesis of Cu-doped ZnO Nanoparticles for Enhanced Photocatalytic Degradation of Methyl Orange: *Applied Surface Science*, 2011, 28(4); 1587-1591.
[54] V. Vaino, G. Lervolino, and L. Rizzo, Cu-doped ZnO as Efficient Photocatalyst for the Oxidataion of Arsenite to Asenate under Visible Light, *Appl. Catal. B Environ,* 2018, 238, 471-479.
[55] P. K. Labhane, V. R. Huse, L. B. Patle, A. L. Chaudhari, and G. H. Sonawane, Synthesis of Cu Doped ZnO Nanoparticles: Crystallographic, Optical, FTIR, Morphological and Photocatalytic Study, *Journal of Material Science and Chemical Engineering*, 2015, 3(7); 39-51.
[56] R. M. Kulkarni, R. S. Malladi, and M. S. Hanagadakar, Cu-ZnO Nanoparticles for Photocatalytic

Degradation of Methyl Orange, *Research Article*, 2018, 3(8), 521-525.
[57] A. L. Birukhait, K. S. Fedlu, M. A. Dinseh, S. G. Noto, K. Dong-Hau, E. M. Chen, D. D. Temesgen and A. Z. Osman, Biogenic Synthesis of Cu-doped ZnO Photocatalyst for the Removal of Organic Dye. *Hindawi Bio-inorganic Chemistry and Application*, 2022, Article ID8081494, 10.
[58] J. Ridwan, J. Yunus, A. A. Umar, A. A. Mohd-Raub, A. A. Hamza, J. Kazmi, A. B. Nandiyanto, R. E. Pawinanto, and I. Hamidah, Vertically Aligned Cu-doped ZnO Nanorods for Photocatalytic Activity Enhancement: *International Journal of Electrochemical Science*, 2022, 17, 220013.
[59] F. A. Ahmed, N. Sheeba, S. B. Meera, G. Manikandan, and M. Yuvashree, Green Synthesis Strategy for Producing Doped and Undoped ZnO Nanoparicles: Their Phototocatalytic Studies for Industrial Dye Degradation, Water Science and Technology, 2021, 84(10); 29-58.
[60] K. Awais, A. Pervaiz, K. Abdulhameed, M. Saleh, U. K. Mayeen, M. D. A. Mottahir, A. Mohd, U. D. Israf, G. C. Ratiram, K. Dileef, S. Rohit, R. I. F. Mohammad, and B. E. Talha, Effect of Cu Doping on ZnO Nanoparticles as a Photocatalyst for the Removal of Organic Wastewater: *Hindawa Bioinorganic Chemistry and Application*, 2022, Article ID 9459886, 12.
[61] F. Z. Nouasria, D. Selloum, A. Henni, S. Tingry, and J. Hrbac, Improvement of the Photocatalytic Performance of ZnO Thin Films in the UV and Sunlight Range by Cu Doping and Additional Coupling with Cu_2O: *Ceramic International*, 2022, 48(9); 13283-13294.
[62] A. S. Aqeel, A. B. Muhammad, T. Aneela, D. C. Ali, A. C. Iftikhar, G. S. Ali, E. C. Seyed, W. Magnus, N. Omer, and H. I. Zafar, Facile Synthesis of Copper-Doped ZnO Nanorods for the Efficient Photodegradation of Methylene Blue and Methyl Orange, *Ceramic International*, 2019, 46(8), 9997-10005.
[63] K. Sini, S. Biswarup, and M. Satyabrata, Highly Efficient Photocatalytic Degradation of Organic Dyes by Cu Doped ZnO Nanostructures, *Phys.Chem.Chem.Phys*, 2015, 17, 25172.
[64] A. H. Yusuf, and U. Gaya, Mechanochemical Synthesis and Characterization of N-Doped TiO_2 for the Photocatalytic Degradation of Caffeine, *Nanochem. Res*, 2018, 3(1), 29-35.
[65] C. Rojas-Michea, M. Morel, F. Garcia, G. Morell, and E. Mosquera, Influence of Copper Doping on Structural Morphological, Optical and Vibrational Properties of ZnO Nanoparticles Synthesized by Sol-gel Method, *Surface and Interfaces*, 2020, 21, Article ID 100700.
[66] J. Vasuderan, S. J. Jeyakumar, B. Arunkumar, M. Jothibas, A. Muthuvel, and S. Vijayalakshmi, Optical and Magnetic Investigation of Cu-doped ZnO Nanoparticles Synthesized by Solid State Method: *Material Today Proceedings*, 2022, 48, 438-442.
[67] N. M. Alatawi, L. Ben Saad, L. Soltane, A. Moulahi, J. Mjejri and F. Sediri, Enhanced Solar Photocatalytic Performance of Cu-doped nanosized ZnO, *Polyhedron*, 2021, 197, 115022.
[68] I. Muz, M. Kurban, Zinc Oxide Nanoclusters and their Potential Applications as CH_4 and CO_2 gas Sensors: Insight from DFT and TD-TDF, *Journal of Computational Chemistry*, 2022, 43(27), 1839-1847.
[69] I. Muz, Enhanced Adsorption of Fluoroquinolone Antibiotic on the Surface of the Mg-, Ca-, Fe- and Zn-doped C_{60} Fulterence: DFT and TD-DFT Approach, *Materiald Today Communications*, 2022, 31, 103798.
[70] M. Kurban, I. Muz, Theoretical Investigation of the Adsorption Behavior of Fluorouracial as an Anticancer Drug on Pristine and B-, Al-, Ga-doped C_{36} Nanotube, *Journal of Molecular Liquids,* 2020, 309, 113209.
[71] I. Muz, M. Kurban, A First Principles Evaluation on the Interaction of 1,3, 4-Oxidiazole with Pristine and B-, Al-,Ga-doped C_{60} Fullerences, *Journal of Molecular Liquids*, 2021, 335, 116181.
[72] I. Muz, F. Goktas, M. Kurban, 3d-transition Metals (Cu, Fe, Mn, Ni, V, and Zn)-doped Pentacene π-Conjugated Organic Molecule for Photovoltaic Applications: DFT and TD-DTF Calculations, *Theoretical Chemistry Accounts*, 2020, 139(2), 23.
[73] L. Anju Chanu, W. Joychandra Singh, K. Jugeshwar Singh, K. Nomita Devi, Effect of Operational Parameters on the Photocatalytic Degradation of Methylene Blue Dye Solution Using Manganese Doped ZnO Nanoparticles: *Results in Physics*, 2019, 12, 1230-1237.
[74] D. Toloman, A. Popa, M. Sten, M. Stefan, G. Vlad, and S. Ulinic, Visible-Light Driven Photocatalytic Degradation of Different Pollutants Using Cu-doped ZnO MWCNT Nanocomposite, *Journal of Alloys and Compound,* 2021, 886, 159010.
[75] P. Suresh, S. Michael, N. Nicholas, G. Miguel, K. Athanassion, H. E. Muhammad, S.M, Patrick, W.J. Jeremy, B. Anthony, O. Kevin, D. D. Dionysios, A Review on the Visible Light Active ZnO Photocatalysts for Environmental Applications: *Chemosphere*, 2012; 125, 331-349.
[76] A. Akhund, and A. Habibi-Yangjeh, Ternaary Magnetic g-C_3N_4/Fe_3O_4/AgI Nanocomposites: Novel Recyclable Photocatalysts with Enhanced Activity in Degradation of Different Pollutants under Visible Ligh: *Material Chemical Physics*. 2016, 174, 59-69.
[77] M. Shellofteh-Gohari, and A. Habibi-Yangjeh, Novel Magnetically Separable Fe_3O_4@ZnO/AgCl Nanocomposites with Highly Enhanced Photocatalytic Activities under Visible Light Irradiation: *Sep Purifi Technol*, 2015, 147, 194-202.
[78] J. Wang, W. J. Jiang, D. Liu, Z. Wei, Y. F. Zhu, Photocatalytic Performance Enhanced via Surface Bismuth Vacancy of $Bi_6S_2O_{15}$ Core/Shell Nanowires: *Applied Catalysis of B Environment*, 2015; 176: 306-314.
[79] N. Huang, J.X. Shu, Z. H. Wang, M. Chen, C. G. Ren, W. Zhang, One Step Pyrolytic Synthesis of ZnO Nanorods with Enhanced Photocatalytic Activity and High Photostability Under Visible and UV Light Irradiation: *Journal of Alloys Compounds*. 2015, 648: 919-929.